

HydraPrompt: An Adaptive and Asymmetric Framework of Vision-Language Models for Synthetic Image Detection

Senyuan Shi^{1*} Hao Tan^{2 4*} Zichang Tan³ Shuhan Feng¹
 Ajian Liu⁴ Sergio Escalera⁵ Jun Wan^{4§}

¹Beijing University of Posts and Telecommunications

²School of Advanced Interdisciplinary Sciences (SAIS), University of Chinese Academy of Sciences

³Shenzhen Institute of Advanced Technology (SIAT), Chinese Academy of Sciences

⁴MAIS, Institute of Automation, Chinese Academy of Sciences

⁵University of Barcelona * Equal contribution, § Corresponding author
 442538552@bupt.edu.cn, {tanhao2023, jun.wan}@ia.ac.cn

Abstract

The rapid evolution of generative models has precipitated a proliferation of fabricated content, posing significant challenges to existing Synthetic Image Detection (SID) methods. Capitalizing on advancements in vision-language models (e.g., CLIP), recent attempts have leveraged learnable textual prompts to identify synthetic images. However, they still leverage static prompt as a fixed boundary for real and fake images, failing to adapt to the varying types of forgery that emerge during inference. To overcome this issue, we propose **HydraPrompt**, an asymmetric prompting framework that dynamically adjusts the category centers by aligning with fine-grained visual cues. Specifically, we propose an Asymmetric Prompt Adapter (APA): (1) for *authentic category*, we introduce a single set of prompts to capture the consistent representative patterns, which serves as a unified anchor for real content. While (2) for *fake category*, we construct sample-adaptive prompts that specialize in capturing diverse cues from different samples, enabling adaptive modeling of forgery image variations. To increase pronounced discriminability within different synthetic images, we further introduce a Conditional Supervised Contrastive (CSC) objective, which compacts the authentic representations while capturing fine-grained forgery clues. Extensive experiments on popular SID benchmarks demonstrate the state-of-the-art performance of our framework.

1 Introduction

Recent years have witnessed the advancement of generative models, such as GANs [19, 34] and LDMs [56]. These models enable the creation of hyper-realistic synthetic images, thus raising wide concerns of potential abuse and privacy threats. In response to these security concerns and privacy threats, a variety of detection methods targeting AI-generated images (AIGIs) have been proposed.

Most existing studies in AIGIs detection [18, 35, 47, 49, 51, 62, 63, 75–77, 80, 83] typically approach it as a symmetric binary classification task, akin to the “cat versus dog” problem. This strategy proves effective in traditional scenarios since the categories exhibit well-defined differences in visual semantics. However, AIGIs tasks focus on fine-grained details rather than high-level visual semantics [37]. In this regard, *authentic images*, despite their diversity, possess a consistent pattern governed by the unified physics of real-world imaging, whereas *synthetic images* contain a wide range of artificial

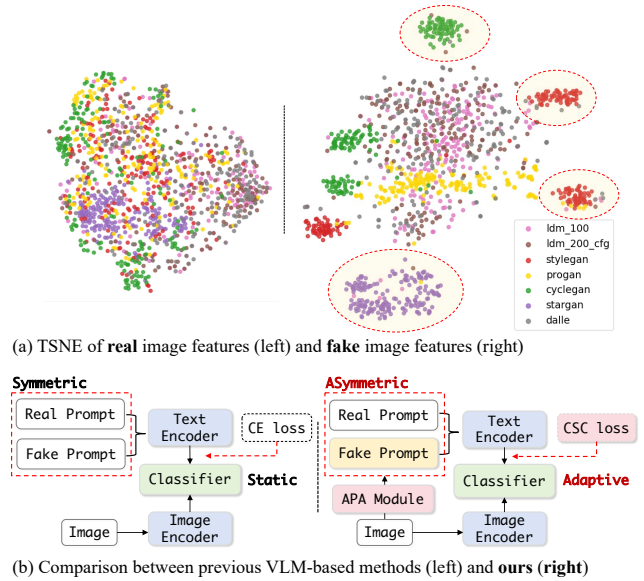


Figure 1: (a) TSNE [45] visualizations of real and fake images on UniversalFakeDetect [49] benchmark. We selected seven subsets from the benchmark. The features are extracted from shallow layers of CLIP ViT-L/14. Real images share a unified distribution while fake images exhibit scattered patterns. (b) Comparison of previous VLM-based strategy and our HydraPrompt. Existing approaches adopt symmetric prompts that produce static category centers. In contrast, HydraPrompt introduces *asymmetric* prompts design to achieve *adaptive* category centers.

patterns due to variations in generative models (e.g., GANs, LDMs) and forgery traces (e.g., structural or physical or even pixel flaws).

Specifically, we visualize the shallow layers image features from pre-trained encoder (Figure 1 (a)), as we hypothesize that the fine-grained details reside in the shallow features of the visual encoder [37]. It can be observed that there is a pronounced distribution shift when confronted with forgery data from different sources. In contrast, real images share a unified distribution, which reflects that there exists an *asymmetric* phenomenon in the AIGIs detection task. Consequently, traditional symmetric strategy raises two crucial limitations: (1) a mismatch between the fixed classification

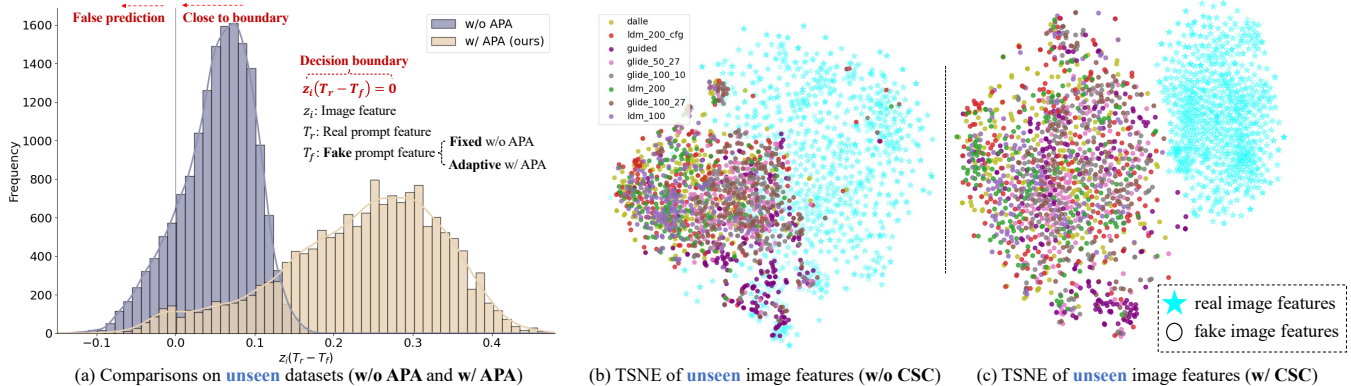


Figure 2: Analyses on the proposed APA and CSC. (a) Effectiveness of APA: $z_i T_r$ and $z_i T_f$ are compared for classification during inference, thus $z_i(T_r - T_f) = 0$ is the decision boundary. The values $z_i(T_r - T_f)$ for fake category are inverted so that positive values indicate correct predictions, and a value close to zero signifies proximity to the boundary (i.e., ambiguous cases). The results reveal that previous strategy is error-prone on unseen data. While the proposed APA constructs adaptive category centers, which increases the margin, leading to improved robustness. (b) and (c) Effectiveness of CSC: we compare the learned image features on unseen subsets from UniversalFakeDetect [49] benchmark. Without CSC, the features of real and fake images exhibit obvious overlap. By contrast, CSC compacts the real representations and prevents the unseen forgeries from collapsing into a narrow region, showing better separability in OOD scenarios.

boundary and the diverse, nuanced visual cues inherent in manipulated content, leading to failures for out-of-distribution (OOD) forgeries. (2) The reliance on fixed classification boundary restricts the model’s ability to adapt to varying types of forgeries, prone to overfitting seen manipulation patterns (as in Figure 2 (b)).

Building on the above investigations, we propose **HydraPrompt**, a conceptually simple yet effective framework based on Vision-Language Models (VLMs), which mitigates the above issues by constructing asymmetric category centers for real and fake classes, as shown in Figure 1 (b).

To address the first issue, we introduce an **Asymmetric Prompt Adapter (APA)**. Unlike existing adapters [42, 62] for SID tasks, which rely on a fixed set of textual prompts, we introduce an asymmetric prompt modeling. Specifically, for real category we employ a single set of prompts to capture the consistent patterns of real-world content. While for the fake category, we introduce sample-adaptive prompts based on fine-grained visual cues, aiming to adapt to diverse clues of forged images. To capture the fine-grained image clues, we explore different methods such as LDR [6] that uses hand-drafted features, and RINE [37] that leverages ensemble of spatial features. We empirically found that the shallow-layer image features coupled with a simple learnable block, can effectively model diverse forged images. As validated in Figure 2 (a), previous strategy is error-prone on unseen data, while our proposed APA greatly improves the classification margin through adaptive modeling of decision boundary, showing great robustness to unseen forgeries.

To mitigate the second issue, we propose **Conditional Supervised Contrastive (CSC)** objective. Specifically, (1) for the image branch, we pull real image features closer toward the unified anchor, while dispersing fake image features to prevent the model from collapsing into seen forgeries. (2) For the text branch, we explicitly separate the text features to preserve their distinctiveness. Additionally, inspired by [71], we introduce an alignment constraint as a regularizer

to align cross-modal representations progressively. As shown in Figure 2 (b) and (c), CSC effectively compacts the representations of real images while dispersing those of fake images, offering better distinctiveness to unseen forgeries. During inference, we compare the cosine similarities between image features and two category centers (i.e., unified real category center and sample-adaptive fake category center) to determine the authenticity.

To sum up, our main contributions are:

- We introduce HydraPrompt, a conceptually simple yet effective framework that dynamically constructs asymmetric prompts to achieve adaptive category centers, achieving substantial gains on popular SID benchmarks.
- We propose **Asymmetric Prompt Adapter (APA)**, which leverages fine-grained visual cues to construct adaptive category centers, enhancing the classification margin statistically on unseen forgeries.
- We propose **Conditional Supervised Contrastive (CSC)** Objective, which facilitates alignment between visual features and asymmetric textual prompts, enhancing the adaptation ability in OOD scenarios.

2 Related Work

2.1 Generalizable Synthetic Image Detection

The evolution of generative models [16, 68, 81] has posed significant security risks to society. Synthetic image detection, which aims to distinguish AI-generated images from authentic images, has become a heated topic. Early studies focus on finding generalizable *features* in different domains, such as spatial domain [18, 47, 49, 63, 75–77, 80], frequency domain [35, 51, 62, 83], time-domain [22–24, 78]

and even model gradients [64]. While the tailored feature extractions fail to generalize well in practical scenarios [79]. Some methods discover that the reconstruction error is a generalizable indicator for synthetic images, hence employing VAE [10, 55] or Denoising U-Net [3, 5, 72] for detection. However, the performance is conditioned on the specific type of VAE and is hard to generalize to GAN-generated images. Some methods aim to mitigate bias in aligned datasets. For instance, [25] [53] align content bias between authentic and synthetic categories through VAE reconstruction, while [7] [12] mitigate frequency bias by further aligning high-frequency information. However, a large amount of bias remains unexplored. Such specific training approaches can make the model prone to overfitting to unseen distributional bias. More recently, some methods [27, 37, 69, 77] take advantage of pre-trained semantics to greatly boost the performance. For instance, Effort [77] utilizes the well-established semantic knowledge to enhance the generalization of synthetic image detection, achieving impressive performance. Although these methods utilize advanced feature extraction strategies, the potential of dynamic category centers is still underexplored.

2.2 VLMs for Synthetic Image Detection

With the developments of Vision-Language Models (VLMs) [41, 52], many attempts tend to ground their capacities into the field of synthetic image detection. For instance, some methods [8, 30, 74, 86] adopt large VLMs for explainable detection, achieving promising results and transparency. Other methods take advantage of CLIP [41]. For example, FatFormer [42] integrates a forgery-aware adapter and dedicated language alignments into CLIP, yielding remarkable performance. C2P-CLIP [61] introduces category common prompts to align the cross-modal embeddings in the forgery space. Sun et al. [60] construct precise forgery explanations to release the potential of CLIP and large VLMs. Lin et al. [38] and Forensics adapter [13] employ learnable prompts to transfer cross-modal knowledge into facial forgery detection. While achieving significant improvements, they still rely on static category centers, neglecting the adaptation capacities of the textual encoder. In this paper, we present an asymmetric cross-modal framework, leveraging fine-grained visual cues to construct dynamic category centers for generalizable forgery detection.

2.3 Prompt Learning for VLMs

Large-scale pre-trained Vision-Language models (VLMs), e.g., CLIP [52] and ALIGN [31] have demonstrated remarkable generalization across various downstream tasks [67, 73], [88–90], [65, 66]. How to efficiently transfer these VLMs into specific domains remains a heated topic. Various methods have been proposed, e.g., prompt learning [85], adapter tuning [20] and LoRA [29]. Among them, the prompt learning technique is widely adopted for its effectiveness and limited computational overhead. Different from hand-crafted textual templates, prompt learning introduces trainable prompt embeddings to facilitate the learning of domain knowledge. For instance, CoOp [85] and CoCoOp [84] introduce learnable textual prompts to transfer CLIP into classification task, yielding impressive few-shot performance. The follow-up works [36, 87] further

improve the generalization abilities either through gradient correction [87], multi-modal prompting [36] or ensemble learning [44]. In this paper, we inherit the merits of learnable prompts, while further incorporating fine-grained visual cues as cross-modal prompts to construct an inference-adaptive framework.

3 Methodology

In this section, we present HydraPrompt, an adaptive and Asymmetric Framework for Synthetic Image Detection. We first define some basic notations and review the classification strategy of CLIP [52]. Then we give a detailed demonstration of our proposed method, including Asymmetric Prompt Adapter (APA) Module, Conditional Supervised Contrastive (CSC) Objective and inference procedure.

3.1 Preliminaries

Notations. Suppose the dataset contains W images, denoted as $\{I_i, \mathbf{y}_i\}_{i=1}^W$. Each image is annotated with a binary label \mathbf{y}_i indicating its authenticity. $\mathbf{y}_i = 0$ represents the image is real and $\mathbf{y}_i = 1$ indicates the image is tampered or entirely generated by AI. Our method is constructed on the CLIP. We denote the image encoder and the text encoder pre-trained from CLIP as $\mathcal{V}(\cdot)$ and $\mathcal{T}(\cdot)$, respectively. **Classification Strategy of CLIP.** Given an input image and candidate labels, the classification is performed by comparing the cosine similarities of the image feature and textual embeddings, where textual embeddings are actually serving as the category centers. Different from traditional vision foundation networks, the semantic knowledge embedded from text encoders are well-aligned with the image feature space. However, the textual embeddings remain static during inference, as in existing SID methods [13, 26], extracted either by hand crafted templates or the learnable prompts, failing to fully release the potential of the text encoder.

3.2 Overall Architecture

With the primary objective of establishing adaptive category centers to ensure that the model maintains strong generalization on unseen data, we introduce two core designs: APA module and CSC objective. As shown in Figure 3, (1) For **APA Module**, we extract the shallow-layer features from the image encoder and integrate learnable prompts to efficiently capture sample-adaptive prompts. (2) For **CSC Objective**, our framework employs two loss functions, where the supervised contrastive loss aligns the intra-modal embeddings comprised both image and text branches, while the alignment constraint handles the cross-modal alignment.

3.3 APA Module

Fine-grained Visual Cues. AIGIs tasks focus on fine-grained visual cues rather than high-level visual semantics. Therefore, we conclude that shallow layers features from image encoder can serve as effective fine-grained visual cues. Specifically, given an input image, we first extract patch embeddings to obtain $Z \in \mathbb{R}^{N \times D}$, where N denotes the number of patches and D represents the embedding dimension. The image encoder processes these embeddings through a sequence of transformer blocks. Let \mathcal{V}_i denote the i -th transformer block in the image encoder. The image features after the first block of image encoder are obtained as: $\tilde{Z} = \mathcal{V}_1(Z)$. Then we apply average pooling over these image features, yielding an

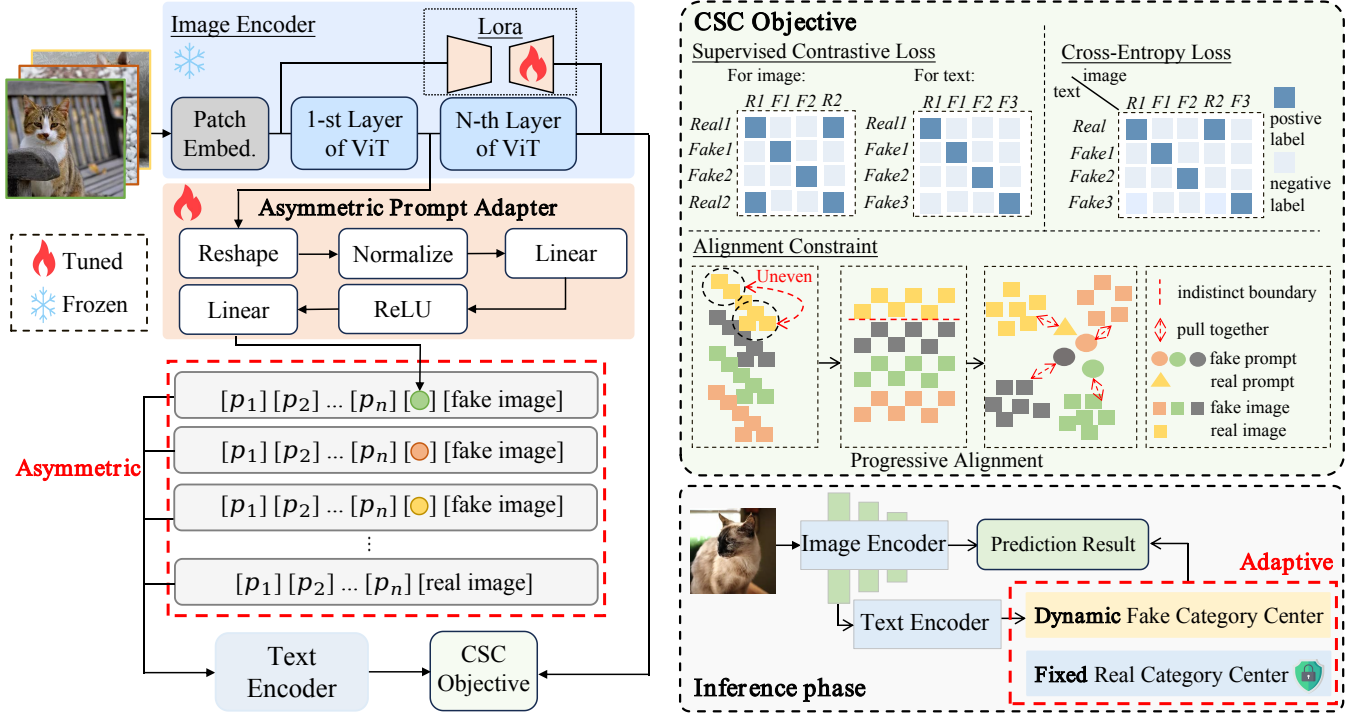


Figure 3: Overview of the proposed HydraPrompt framework. During training phase, we design sample-adaptive prompts for fake image features, while using a single set of learnable prompts for real image features. P_n denotes the learnable prompts. The CSC objective is employed to align both intra-modal and cross-modal embedding space. In inference phase, we obtain real logit by calculating the cosine similarity between image features and fixed real text prompts, and the fake logit by calculating the cosine similarity between image features and adaptive prompts. (1) Asymmetric: the distinct design of textual embeddings for different categories. (2) Adaptive: fine-grained visual cues of test image are extracted as part of sample-adaptive prompts, enabling the achievement of adaptive category centers.

aggregate representation as:

$$\hat{Z} = \frac{1}{N} \sum_{i=1}^N \tilde{z}_i, \quad \tilde{z}_i \in \mathbb{R}^D. \quad (1)$$

Then, we employ a lightweight learnable adapter to project the extracted features \hat{Z} . The process can be formulated as:

$$\tilde{Z} = W_2^T (\text{ReLU}(W_1^T \hat{Z} + b_1)) + b_2, \quad (2)$$

where $W_1 \in \mathbb{R}^{D \times D'}$ and $W_2 \in \mathbb{R}^{D' \times D}$ are trainable weights with $D' < D$. b_1 and b_2 are bias terms. \tilde{Z} is the modulated feature containing fine-grained visual cues.

Construction of adaptive category centers. To address the mismatch between fixed classification boundary and diverse, nuanced visual cues in manipulated content, we introduce sample-adaptive prompts based on the fine-grained visual cues. Specifically, we construct **two** sets of textual embeddings for each input image. Firstly, we employ learnable prompts $P_r \in \mathbb{R}^{M \times D}$ to extract a consistent textual embedding, where M denotes the number of prompts. This remains static during inference, serving as a stable anchor for authentic images. Secondly, we take fine-grained visual cues \tilde{Z} as a cross-modal prompt, together with another set of learnable prompts $P_f \in \mathbb{R}^{M \times D}$ to construct sample-adaptive textual embeddings. The

above process can be written as:

$$\begin{aligned} T_r &= \mathcal{T}([P_r, C_r]), \\ T_f &= \mathcal{T}([P_f, \tilde{Z}, C_f]), \end{aligned} \quad (3)$$

where C_r is the context vector obtained from the text ‘‘A real image’’ and C_f is the context vector obtained from ‘‘A fake image’’, serving as the common anchors for the corresponding categories. T_r is the unified textual embeddings for authentic category and T_f is the sample-adaptive textual embeddings for synthetic category. $[\cdot]$ denotes concatenation operation. Conditioning on fine-grained visual cues, T_f is capable of constructing sample-adaptive prompts, effectively adapting the category centers.

3.4 CSC Objective

Supervised Contrastive Objective. Based on the asymmetric architecture, we encourage the features of the real class to cluster together, while the features of the fake class remain dispersed. The process can be formulated as:

$$\mathcal{L}_{sc}^I = \frac{1}{B} \sum_{i=1}^B \frac{-1}{\sum_{j=1}^B M_{ij}} \log \frac{\sum_{j=1}^B M_{ij} e^{(z_i \cdot z_j / \tau)}}{\sum_{k=1}^B e^{(z_i \cdot z_k / \tau)}}, \quad (4)$$

$$\mathbf{M}_{ij} = \begin{cases} 1, & \text{if } \mathbf{y}_i = 0 \text{ and } \mathbf{y}_j = 0, \\ 1, & \text{if } \mathbf{y}_i = 1 \text{ and } i = j, \\ 0, & \text{otherwise,} \end{cases} \quad (5)$$

$$\mathcal{L}_{sc} = \frac{1}{2} (\mathcal{L}_{sc}^I + \mathcal{L}_{sc}^T), \quad (6)$$

where B denotes the batch size, and \mathbf{z}_i represents the normalized feature of the i -th image in the batch. \mathcal{L}_{sc}^I and \mathcal{L}_{sc}^T refer to the image and text branch, which share the analogous formula in the supervised contrastive objective. The temperature parameter τ controls the sharpness of the similarity distribution. The mask matrix $\mathbf{M} \in \{0, 1\}^{B \times B}$ defines positive pairs for the supervised contrastive objective. There are two strategies: (1) ‘‘individual’’, this strategy denotes that each feature is regarded as an individual by pushing the feature apart from one another. (2) ‘‘cluster’’, this strategy denotes all features are regarded as a single cluster by pulling them together. In our framework, we employ a ‘‘cluster’’ strategy for the authentic category and an ‘‘individual’’ strategy for the synthetic category as shown in Eq. 5.

Alignment Constraint. To further enhance the construction of adaptive category centers, we incorporate an alignment constraint for cross-modal alignment. Inspired by [71], we formulate the alignment constraint as follows:

$$\mathcal{L}_{\text{align}} = \frac{1}{B} \sum_{i=1}^B \frac{-1}{\sum_{j=1}^B \mathbf{M}_{ij}} \log \frac{\sum_{j=1}^B \mathbf{M}_{ij} e^{(\mathbf{z}_i \cdot \mathbf{t}_j^T / \tau)}}{\sum_{k=1}^B e^{(\mathbf{z}_i \cdot \mathbf{t}_k^T / \tau)}}, \quad (7)$$

where \mathbf{t}_j^T denotes the normalized features of the j -th text in the batch. The mask matrix \mathbf{M} is the same as Eq. 5. This term pulls positive pairs closer, aligning real representations and sample-adaptive fake representations progressively.

Classification. Finally, we introduce a classification loss \mathcal{L}_{cls} , which is a variant of standard cross-entropy loss adapted to asymmetric prompting framework. Specifically, there are two output logits $\{o_r^i, o_f^i\}$ for the i^{th} input. The first one is computed from the static embedding T_r while the second is based on sample-adaptive embedding T_f^i :

$$o_r^i = \mathbf{z}_i \cdot T_r, o_f^i = \mathbf{z}_i \cdot T_f^i. \quad (8)$$

The classification loss can be calculated as:

$$\mathcal{L}_{\text{cls}} = - \sum_{i=1}^B \left(\mathbf{y}_i \log \left(\frac{e^{o_f^i}}{e^{o_f^i} + e^{o_r^i}} \right) + (1 - \mathbf{y}_i) \log \left(\frac{e^{o_r^i}}{e^{o_r^i} + e^{o_f^i}} \right) \right). \quad (9)$$

Final Objective. The overall loss function combines the classification loss, supervised contrastive loss, and the alignment constraint with their respective hyperparameters:

$$\mathcal{L} = \mathcal{L}_{\text{cls}} + \lambda_1 \mathcal{L}_{sc} + \lambda_2 \mathcal{L}_{\text{align}}, \quad (10)$$

where λ_1 and λ_2 are coefficients that balance the importance of the corresponding regularization term.

3.5 Inference

During the inference stage, there are two candidate centers for each input image, i.e., T_r and T_f calculated by Eq. 3. Then we calculate their distance to the current image by using Eq. 8. By comparing the distances (i.e., o_r^i and o_f^i), we can determine the authenticity of the current input image.

4 Experiments

4.1 Implementation Details

We utilize CLIP ViT-L/14 [52] as the default vision-language model. The input images are first resized to 256×256 resolutions, and then cropped into 224×224 resolutions. No further data augmentations are performed during training phase. λ_1, λ_2 are set to 1 and 1.25. The model is trained for 10 epochs with a learning rate of $4e - 4$ and decays with cosine policy. To ensure a sufficient number of negative samples, we adopt the standard memory bank mechanism which stores and updates sample representations across training iterations. Therefore, the batch size can be increased to 1000 on a single RTX 4090 GPU. LoRA is integrated into the MLPs of all layers with rank 6 and alpha 6. The corresponding experiments are provided in the supplementary material.

4.2 Datasets and Metrics

We conducted experiments on three popular SID benchmarks: UniversalFakeDetect [49], Chameleon [75], and WildRF [2]. (1) For **UniversalFakeDetect** benchmark, we adhere to the protocol outlined in [49] and utilize ProGAN as our training dataset, which includes 20 subsets of generated images. For evaluation, we follow the testing GANs datasets setting [1, 9, 11, 19, 33, 50, 58] and diffusion model datasets setting [14, 48, 54, 57] in FatFormer [42]. Following existing work [42], we report both average precision (AP) and classification accuracy (Acc). For Acc, we set the classification threshold for each dataset at 0.5 to ensure fair comparison. (2) For **Chameleon** dataset, which contains widespread post-processing artifacts and is designed to evaluate model performance on challenging data, we adhere to the protocol outlined in [75] and adopt two training settings: one using ProGAN [19] and the other using SD v1.4 [28]. Following existing work [75], we report the Acc metric. (3) For **WildRF** dataset, which aims to address the difficulty of AIGIs detection in online environments, we adhere to the protocol outlined in [2], and the test datasets include Reddit, Twitter, Facebook. We report the Acc metric.

4.3 Main Results

Comparison on UniversalFakeDetect benchmark. We choose several previously popular methods, including [15, 17, 37, 42, 49, 51, 61, 62, 64, 70, 77] as shown in Table 1 for comparison with our method. Compared with other prompt-based VLM approaches, such as (1) FatFormer [42], which designs a forgery-aware adapter and a text-guided interactor, our method achieves a cumulative performance improvement of 1.9% and 3.1% on GANs and Diffusion model datasets. Similarly, (2) C2P-CLIP [61], which injects category concepts into the image encoder through the text encoder, our method achieves gains of 2.7% and 2.9%, respectively. Beyond prompt-based VLM approaches, such as RINE [37], which exploits fine-grained visual cues as discriminative elements, our method achieves a cumulative improvement of 2.6% and 5.5%, respectively. Effort [77], which explicitly constructs the orthogonal semantic and forgery subspaces via singular value decomposition (SVD), our method achieves an additional gain of 0.7% and 1.6%, respectively. This performance on unseen generators supports the effectiveness and robustness of our framework.

Methods	ProGAN	StyleGAN	BigGAN	CycleGAN	GauGAN	StarGAN	Deepfake	Mean
CNNSpot [70]	64.6 / 92.7	52.8 / 82.8	51.6 / 70.5	58.6 / 81.5	51.2 / 74.3	53.6 / 86.6	50.6 / 51.5	57.3 / 79.6
Durall [15]	79.0 / 73.9	63.6 / 58.8	69.5 / 62.9	65.4 / 60.8	99.4 / 99.4	67.0 / 63.0	50.5 / 50.2	70.2 / 66.4
Frank [17]	85.7 / 81.3	73.1 / 68.5	76.9 / 70.8	86.5 / 80.8	85.0 / 77.0	67.3 / 65.3	50.1 / 55.3	75.0 / 71.2
F3Net [51]	97.9 / 100	84.5 / 99.5	65.5 / 73.4	81.2 / 89.7	100 / 100	57.0 / 59.2	59.9 / 83.0	78.5 / 88.1
LGrad [64]	99.8 / 100	94.8 / 99.7	82.5 / 92.4	85.9 / 94.7	99.7 / 99.9	73.7 / 83.2	60.6 / 67.8	86.2 / 92.2
UnivFD [49]	99.7 / 100	78.8 / 97.4	91.2 / 99.0	91.9 / 99.8	96.3 / 99.9	91.9 / 100	80.0 / 89.4	88.1 / 97.8
FreqNet [62]	97.9 / 99.6	97.6 / 99.9	90.5 / 96.1	95.8 / 99.5	90.2 / 99.7	93.4 / 98.6	97.4 / 99.9	94.7 / 99.0
RINE [37]	100 / 100	99.3 / 100	99.6 / 99.9	88.9 / 99.4	99.5 / 100	99.8 / 100	80.6 / 97.9	95.4 / 99.6
FatFormer [42]	99.8 / 100	99.9 / 100	98.9 / 99.9	87.7 / 97.4	100 / 100	99.9 / 100	89.4 / 97.3	96.5 / 99.2
C2P-CLIP [61]	99.7 / 100	99.4 / 100	95.3 / 99.9	90.7 / 99.9	95.3 / 100	96.6 / 100	89.9 / 97.3	95.3 / 99.6
Effort [77]	100 / 100	95.1 / 100	99.6 / 99.9	99.9 / 97.7	99.6 / 100	100 / 100	87.6 / 98.9	97.4 / 99.5
HydraPrompt (Ours)	99.9 / 100	96.9 / 100	98.8 / 99.8	98.2 / 99.9	98.4 / 100	100 / 100	93.7 / 97.5	98.0 / 99.6

Table 1: Accuracy and average precision comparisons with state-of-the-art methods in GANs datasets on UniversalFakeDetect [49] benchmark. We report the performance in the formulation of Acc / AP. The best results are highlighted in bold.

Methods	Guided	DALL-E	LDM 200 steps	LDM 200 w/cfg	LDM 100 steps	Glide 100-27	Glide 50-27	Glide 100-10	Mean
CNNSpot [70]	54.9 / 66.6	51.8 / 61.3	52.0 / 64.5	51.6 / 63.1	51.9 / 63.7	53.0 / 71.3	54.2 / 76.0	53.3 / 72.9	52.4 / 70.1
Durall [15]	40.6 / 42.3	55.9 / 58.0	61.7 / 61.7	58.4 / 58.5	62.0 / 62.6	48.9 / 46.9	51.7 / 49.9	54.9 / 52.3	51.7 / 51.8
Frank [17]	53.4 / 52.5	57.0 / 62.5	56.4 / 50.9	56.5 / 52.1	56.6 / 51.3	50.4 / 40.8	52.0 / 42.3	53.6 / 44.3	53.2 / 50.2
F3Net [51]	69.2 / 70.8	71.6 / 79.9	73.4 / 83.3	80.7 / 89.1	74.1 / 84.0	87.0 / 94.5	88.5 / 95.4	88.3 / 95.4	80.6 / 89.2
LGrad [64]	86.6 / 100	88.5 / 97.3	94.2 / 99.1	95.9 / 99.2	94.8 / 99.2	87.4 / 95.1	90.7 / 95.1	89.4 / 94.9	89.4 / 97.7
UnivFD [49]	75.7 / 85.1	89.5 / 96.8	90.2 / 97.1	77.3 / 88.6	90.5 / 97.0	90.7 / 97.2	91.1 / 97.4	90.1 / 97.0	85.4 / 94.6
FreqNet [62]	86.7 / 96.3	59.1 / 77.8	84.6 / 96.1	99.6 / 100	65.6 / 62.3	85.7 / 99.8	97.4 / 99.8	88.2 / 96.4	83.4 / 91.1
RINE [37]	76.1 / 96.4	95.0 / 99.3	98.3 / 99.8	88.2 / 98.3	98.6 / 99.9	88.9 / 93.8	92.6 / 99.3	90.7 / 98.9	91.1 / 98.8
FatFormer [42]	76.1 / 92.0	98.8 / 99.8	98.6 / 99.8	94.9 / 99.1	98.7 / 99.9	94.4 / 99.1	94.7 / 99.4	94.2 / 99.2	93.8 / 98.5
C2P-CLIP [61]	69.1 / 92.2	98.6 / 99.9	99.3 / 100	97.3 / 99.8	99.3 / 100	95.3 / 99.3	95.3 / 99.3	96.1 / 99.4	93.8 / 98.7
Effort [77]	69.2 / 95.4	98.1 / 99.9	99.3 / 99.9	96.8 / 99.9	99.5 / 100	97.5 / 99.9	97.8 / 99.9	97.2 / 99.9	94.4 / 99.4
HydraPrompt (Ours)	89.5 / 97.6	98.4 / 99.9	99.5 / 100	97.3 / 99.9	99.6 / 100	93.7 / 99.4	95.4 / 99.6	93.7 / 99.7	95.9 / 99.5

Table 2: Accuracy and average precision comparisons with state-of-the-art methods in diffusion model datasets on Universal-FakeDetect [49] benchmark. We report the performance in the formulation of Acc / AP. The best results are highlighted in bold.

Training Data	CNNSpot	FreDect	Fusing	GramNet	LNP	UnivFD	DIRE	PatchCraft	NPR	AIDE	HydraPrompt (Δ)
ProGAN [19]	56.9 0.1/99.7	55.6 13.7/87.1	57.0 0.0/99.8	58.9 4.8/99.7	57.1 0.1/99.9	57.2 3.2/97.8	58.2 3.3/99.5	53.8 1.8/92.8	57.3 2.2/98.7	58.4 5.0/98.5	61.3 (+2.4) 31.6/83.7
SD v1.4 [28]	60.1 8.9/98.6	56.9 1.4/98.6	57.1 0.0/99.9	61.0 17.7/93.5	55.6 0.6/97.0	55.6 75.0/44.1	59.7 11.9/95.7	56.3 3.1/96.4	59.1 2.4/100.0	62.6 20.3/94.4	69.7 (+7.1) 37.9/93.9

Table 3: Accuracy comparisons with previous state-of-the-art methods on Chameleon [75] dataset. The first row indicates accuracy (Acc) evaluated on Chameleon test dataset, and the second row gives the Acc for “fake image / real image” for detailed analysis. “ Δ ” denotes the performance improvement compared with previous best method and are highlighted in red. The best results are highlighted in bold.

Methods	Facebook	Reddit	Twitter	Mean
CNNSpot [70]	70.6	75.4	71.4	72.5
PatchFor [4]	77.1	87.8	81.6	82.2
UnivFD [49]	78.4	80.8	78.1	79.1
NPR [63]	76.6	89.8	79.5	81.9
LaDeDa [2]	81.9	91.8	83.3	85.7
HFMF [46]	86.9	92.3	85.8	89.4
HydraPrompt (Ours)	95.2	95.3	97.3	95.9
Δ Prev. Best	+8.3	+3.0	+11.5	+6.5

Table 4: Accuracy comparisons with previous state-of-the-art methods on WildRF [2] dataset. All methods are trained on the WildRF training set and evaluated on the three subsets of the WildRF test datasets. We report the performance in the formulation of Acc. The best results are highlighted in bold, the gains are in red.

Comparison on Chameleon dataset. We choose several previously popular methods, including CNNSpot [70], FreDect [17], Fusing [32], GramNet [43], LNP [40], UnivFD [49], DIRE [72], PatchCraft

[82], NPR [63], AIDE [75] for comparison with our method. Note that in the case of widespread post-processing artifacts and challenging test samples in Chameleon dataset, our method achieves an accuracy of over 60% under ProGAN training setting, achieving an improvement of 2.4% respectively. Under SD v1.4 training setting, our method still achieves improvements of 7.1% respectively, with an accuracy approaching 70%.

Comparison on WildRF dataset. This is a dataset curated from several popular social networks, dedicated to evaluating model performance in online environments. We choose several previous popular methods, including [2, 4, 46, 49, 63, 70] as shown in Table 4. It is noteworthy that in the online environments, our method still achieves over 90% accuracy under the WildRF training setting, with an improvement of 8.3%, 3.0% and 11.5% on these three test datasets compared with previous best methods, respectively.

Metric	UniFD[49]	WildRF[2]	LOKI[21]	MSCOCO[39]	Avg.
Acc	98.8	95.7	91.6	98.9	96.3

Table 5: Quantitative analysis (%) of stability for the static prompt for high-variance authentic images. Specifically, LOKI[21] contains proprietary real images such as medicine and remote sensing, while MSCOCO[39] covers the distribution of the vast majority of real-world imagery.

Method	Acc	AP	Avg.
CoOp[85]	92.1	97.5	94.8
CoCoOp[84]	90.8	96.0	93.4
HydraPrompt	94.7	98.2	96.5
Δ CoOp baseline	(+2.6)	(+0.7)	(+1.7)

Table 6: Performance comparison (%) with similar prompt-tuning method. It can be observed that in SID task, HydraPrompt’s performance is significantly superior. Therefore, the asymmetric design of HydraPrompt reflects a principled modeling choice rather than an empirical refinement of existing prompt-tuning strategies.

Metrics	bs	CoOp	CoCoOp	FatFormer[42]	HydraPrompt
FLOPs(G)	1	94.55	94.55	127.95	94.56
	8	664.76	756.44	1023.63	710.61(-313.02)
Latency(ms)	1	28.98	31.96	125.37	32.42
	8	59.63	65.19	216.76	63.17(-153.59)

Table 7: Quantitative analysis of the computational overhead of HydraPrompt and several previous popular methods. “bs” refers to batch size.

4.4 Analysis and Ablation Study

We conduct the following analysis and ablation studies to comprehensively evaluate the effectiveness of each component of our framework. Unless specified, we report the mean of Acc and AP of the GANs and Diffusion model setting on UniversalFakeDetect [49] benchmark.

Robustness of a single set of prompts for authentic images.

To analyze this, we conduct additional evaluations on diverse real datasets in Table 5. The SID tasks primarily focus on fine-grained details. In this regard, real images possess a consistent distribution by the unified physics of real-world imaging. This physical invariance allows a static prompt to effectively anchor the real distribution, even across vast semantic variations.

Robustness of adaptive prompts for fake images. Qualitatively, we selected the unseen subsets from the UniversalFakeDetect[49] benchmark in Figure 4. It shows the overall fake text and image features are consistently more closely aligned, while maintaining a distinct decision boundary from the real class distribution. This suggests that the distribution of adaptive prompts is highly regularized under the CSC objective.

Performance compared with similar prompt-tuning method.

We strictly reproduce the CoOp and CoCoOp algorithms and conduct the following experiments in Table 6. The SID tasks primarily focus on fine-grained details. In this regard, SID is intrinsically asymmetric, distinguishing it from the general semantic tasks associated with CoCoOp. An adaptive prompt for the real class may disrupt the unified physical distribution of real-world imaging.

Computational overhead. We calculate the computational overhead of HydraPrompt and several previous popular methods in

visual cues	Type	Acc	AP	Avg.
Layer 1	Low-level	96.9	99.6	98.2
Layer 12	Mid-level	94.2	99.0	96.6 (-1.6)
Layer 24	High-level	91.4	98.0	94.7 (-3.5)
LDR-Net [6]	Frequency	95.3	97.8	96.5 (-1.7)
RINE [37]	Ensemble	95.4	98.8	97.1 (-1.1)

Table 8: Quantitative analysis (%) of fine-grained visual cues in APA Module. We adopt Layer 1 setting in HydraPrompt.

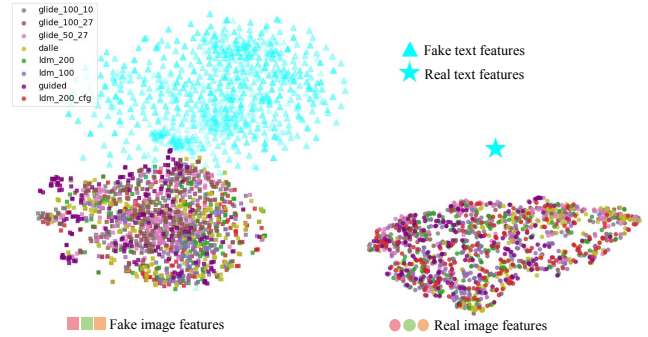


Figure 4: TSNE of Hydraprompt on unseen subsets from UniversalFakeDetect [49] benchmark in cross-modal embedding.

Table 7, and the results show that HydraPrompt has relatively higher computational efficiency.

Quantitative analysis of fine-grained visual cues in APA Module.

In Table 8, we compare different strategies for extracting fine-grained visual cues, including shallow (layer 1), middle (layer 12), and deep (layer 24) features from image encoder, the hand-crafted local cues based on neighboring pixel variations proposed by LDR-Net [6] and the approach of RINE [37], which concatenates CLS tokens from all encoder layers by a fully connected layer. The experimental results demonstrate that under our APA Module and CSC Objective, using features from the first layer of image encoder achieves the best performance.

Ablation on the APA designs. In Table 9a, we compare the impact of different prompt configurations on model performance. “Ada.” refers to sample-adaptive prompt, which incorporates fine-grained visual cues, while static denotes a single set of learnable prompts. The baseline (i.e., “Real-Static” and “Fake-Static”) achieves 91.5% Acc and 96.7% AP. Compared to this baseline, the incorporation of our APA Module significantly improves the performance, with gains of 5.4% in Acc and 2.9% in AP. Note that *when both the real and fake prompts are set to “Ada.”, the model fail to yield a relative performance improvement.* As shown in Figure 1, an asymmetric phenomenon exists in the SID task, leading these symmetric text prompts, although dynamic, to fail in providing an effective adaptive category center.

Ablation on CSC objective designs. In Table 9b, we compare different combinations of the CSC objective. “Ind.” denotes that each feature is regarded as an individual by pushing the feature apart from one another. “Clus.” denotes all features are regarded as a single cluster by pulling them together. Under our APA Module, the baseline (i.e., “Real-Cluster” and “Fake-Cluster”) achieves 94.7% Acc and 98.2% AP. On this basis, our proposed objective further improves the performance by 2.2% in Acc and 1.4% in AP. In Table 9c,

Real		Fake		Acc	AP	Avg.
Ada.	Static	Ada.	Static			
✓			✓	89.2	96.1	92.6
✓		✓		90.2	95.7	92.9
	✓		✓	91.5	96.7	94.1
	✓	✓		96.9	99.6	98.2
△ Baseline				+5.4	+2.9	+4.1

(a) Ablation (%) on prompts design in APA Module. “Ada.” denotes Adaptive. The baseline is “Real-Static” and “Fake-Static” setting.

Real		Fake		Acc	AP	Avg.
Ind.	Clus.	Ind.	Clus.			
✓			✓	92.9	99.3	96.1
✓		✓		90.2	95.4	92.8
	✓		✓	94.7	98.2	96.5
	✓	✓		96.9	99.6	98.2
△ Baseline				+2.2	+1.4	+1.7

(b) Ablation (%) of M_{ij} on CSC Objective. “Ind.”, “Clus.” denotes Individual and Cluster. The baseline is “Real-Clus.” and “Fake-Clus.” setting.

\mathcal{L}_{sc}		Acc	AP	Avg.
text	image			
✓	×	92.2	96.8	94.5
×	✓	94.1	98.0	96.1
✓	✓	96.9	99.6	98.2

(c) Ablation (%) on \mathcal{L}_{sc} design on CSC Objective. We adopt text and image branches setting.

Table 9: Ablation (%) experiments for HydraPrompt. We choose three ablation studies below, including prompt design in APA Module (a), M_{ij} on CSC Objective (b), and \mathcal{L}_{sc} design on CSC Objective (c). Default settings are marked in gray.

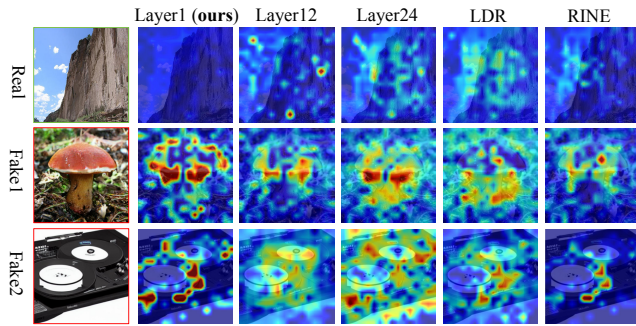


Figure 5: Qualitative analysis of fine-grained visual cues by gradient norm [59] visualization, which is trained with five different designs in APA, including the shallow layer (Layer 1), middle layer (layer 12), deep layer (Layer 24) of image encoder, along with two previous popular methods (i.e., LDR-net [6]), RINE [37]. We select the gradient norm based on the logit of fake class, therefore, a higher value indicates greater attention to forgery artifacts. The layer 1 setting is adopted in our HydraPrompt.

we compare different combinations of the \mathcal{L}_{sc} . The experiments show that applying the \mathcal{L}_{sc} to different branches has a certain impact on the model’s performance, and the optimal performance is achieved when the \mathcal{L}_{sc} is applied to both the text and image branches simultaneously.

4.5 Further Analysis

Qualitative analysis of fine-grained visual cues in APA Module. We visualize the gradient norm [59] maps of forgery traces under different strategies in Figure 5. Our framework adopts the strategy of Layer 1. (1) For authentic category, the models built with Layer 1 exhibit less attention to forgery traces, whereas others exhibit unreasonable attention patterns. (2) For synthetic category, the models built with shallow layer features (Layer 1) focus more on key regions, such as the structure and contours of the mushroom in “Fake 1”, and the shape and edges of the disc in “Fake 2”. In contrast, models built with deeper features (Layer 24) and frequency domain fingerprints (LDR-Net [6]) exhibit more dispersed attention areas and are relatively weaker in capturing crucial information. Based on this, we conclude that shallow layers of image encoder capture fine-grained details, which are more crucial in SID task, thereby enabling the model to learn more effective representations.

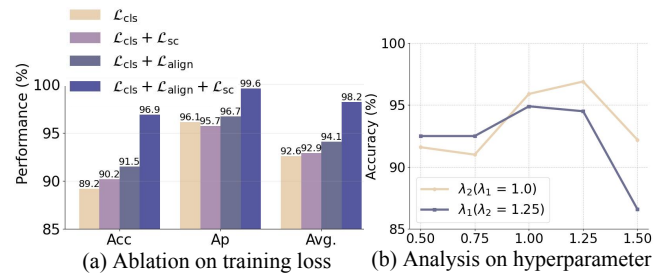


Figure 6: (a) Ablation (%) on training loss design, including \mathcal{L}_{cls} , \mathcal{L}_{sc} , \mathcal{L}_{align} . (b) Analysis of hyperparameter.

Ablation on training loss. We compare different combinations of training loss in Figure 6 (a). The results demonstrate that the model achieves optimal performance when both \mathcal{L}_{align} and \mathcal{L}_{sc} are incorporated. It can be observed that adding only one of them has a limited impact on performance, as \mathcal{L}_{sc} focuses on the intra-modal features alignment, while \mathcal{L}_{align} operates on the cross-modal features alignment. Therefore, the model can learn more effective representations when these two constraints work collaboratively.

Sensitivity analysis of the parameters λ_1 and λ_2 on training loss. We select different combinations of λ_1 and λ_2 on validation sets of UniversalFakeDetect [49] benchmark in Figure 6 (b), it can be observed that these hyperparameters also have a noticeable impact on the experimental results. It shows the optimal performance can be achieved when λ_1 is set to 1.0 and λ_2 is set to 1.25.

5 Conclusion

In this paper, we propose HydraPrompt, an adaptive and asymmetric prompting framework that achieves adaptive category centers during inference. It employs an APA module for constructing sample-adaptive prompts, supported by a CSC objective to boost adaptation ability. Experiments on popular SID benchmarks from distinct perspectives demonstrate the state-of-the-art performance of HydraPrompt.

References

- [1] Andrew Brock, Jeff Donahue, and Karen Simonyan. 2018. Large scale GAN training for high fidelity natural image synthesis. *arXiv preprint arXiv:1809.11096* (2018).
- [2] Bar Cavia, Eliahu Horwitz, Tal Reiss, and Yedid Hoshen. 2024. Real-time deepfake detection in the real-world. *arXiv preprint arXiv:2406.09398* (2024).
- [3] George Cazenavette, Avneesh Sud, Thomas Leung, and Ben Usman. 2024. Fakeinversion: Learning to detect images from unseen text-to-image models by inverting stable diffusion. In *Proceedings of the IEEE/CVF Conference on Computer*

- Vision and Pattern Recognition*. 10759–10769.
- [4] Lucy Chai, David Bau, Ser-Nam Lim, and Phillip Isola. 2020. What makes fake images detectable? understanding properties that generalize. In *European conference on computer vision*. Springer, 103–120.
 - [5] Baoying Chen, Jishen Zeng, Jianquan Yang, and Rui Yang. 2024. Drct: Diffusion reconstruction contrastive training towards universal detection of diffusion generated images. In *Forty-first International Conference on Machine Learning*.
 - [6] JiaXin Chen, Miao Hu, DengYong Zhang, Yun Song, and Xin Liao. 2025. LDR-Net: A Novel Framework for AI-generated Image Detection via Localized Discrepancy Representation. *arXiv preprint arXiv:2501.13475* (2025).
 - [7] Ruoxin Chen, Junwei Xi, Zhiyuan Yan, Ke-Yue Zhang, Shuang Wu, Jingyi Xie, Xu Chen, Lei Xu, Isabel Guan, Taiping Yao, et al. 2025. Dual Data Alignment Makes AI-Generated Image Detector Easier Generalizable. *arXiv preprint arXiv:2505.14359* (2025).
 - [8] Yize Chen, Zhiyuan Yan, Guangliang Cheng, Kangran Zhao, Siwei Lyu, and Baoyuan Wu. 2024. X2-dfd: A framework for explainable and extendable deepfake detection. *arXiv preprint arXiv:2410.06126* (2024).
 - [9] Yunje Choi, Minje Choi, Munyoung Kim, Jung-Woo Ha, Sunghun Kim, and Jaegul Choo. 2018. Stargan: Unified generative adversarial networks for multi-domain image-to-image translation. In *Proceedings of the IEEE conference on computer vision and pattern recognition*. 8789–8797.
 - [10] Beilin Chu, Xuan Xu, Xin Wang, Yufei Zhang, Weike You, and Linna Zhou. 2025. Fire: Robust detection of diffusion-generated images via frequency-guided reconstruction error. In *Proceedings of the Computer Vision and Pattern Recognition Conference*. 12830–12839.
 - [11] Casey Chu, Andrey Zhmoginov, and Mark Sandler. 2017. Cyclegan, a master of steganography. *arXiv preprint arXiv:1712.02950* (2017).
 - [12] Riccardo Corvi, Davide Cozzolino, Ekta Prashnani, Shalini De Mello, Koki Nagano, and Luisa Verdoliva. 2025. Seeing What Matters: Generalizable AI-generated Video Detection with Forensic-Oriented Augmentation. *arXiv preprint arXiv:2506.16802* (2025).
 - [13] Xinjie Cui, Yuezun Li, Ao Luo, Jiaran Zhou, and Junyu Dong. 2025. Forensics adapter: Adapting clip for generalizable face forgery detection. In *Proceedings of the Computer Vision and Pattern Recognition Conference*. 19207–19217.
 - [14] Prafulla Dhariwal and Alexander Nichol. 2021. Diffusion models beat gans on image synthesis. *Advances in neural information processing systems* 34 (2021), 8780–8794.
 - [15] Ricard Durall, Margret Keuper, and Janis Keuper. 2020. Watch your up-convolution: Cnn based generative deep neural networks are failing to reproduce spectral distributions. In *Proceedings of the IEEE/CVF conference on computer vision and pattern recognition*. 7890–7899.
 - [16] Patrick Esser, Sumith Kulal, Andreas Blattmann, Rahim Entezari, Jonas Müller, Harry Saini, Yam Levi, Dominik Lorenz, Axel Sauer, Frederic Boesel, et al. 2024. Scaling rectified flow transformers for high-resolution image synthesis. In *Forty-first international conference on machine learning*.
 - [17] Joel Frank, Thorsten Eisenhofer, Lea Schönherr, Asja Fischer, Dorothea Kolossa, and Thorsten Holz. 2020. Leveraging frequency analysis for deep fake image recognition. In *International conference on machine learning*. PMLR, 3247–3258.
 - [18] Xinghe Fu, Zhiyuan Yan, Taiping Yao, Shen Chen, and Xi Li. 2025. Exploring unbiased deepfake detection via token-level shuffling and mixing. In *Proceedings of the AAAI Conference on Artificial Intelligence*, Vol. 39. 3040–3048.
 - [19] Hongchang Gao, Jian Pei, and Heng Huang. 2019. Progan: Network embedding via proximity generative adversarial network. In *Proceedings of the 25th ACM SIGKDD international conference on knowledge discovery & data mining*. 1308–1316.
 - [20] Peng Gao, Shijie Geng, Renrui Zhang, Teli Ma, Rongyao Fang, Yongfeng Zhang, Hongsheng Li, and Yu Qiao. 2024. Clip-adapter: Better vision-language models with feature adapters. *International Journal of Computer Vision* 132, 2 (2024), 581–595.
 - [21] Harshayu Girase, Haiming Gang, Srikanth Malla, Jiachen Li, Akira Kanehara, Karttikeya Mangalam, and Chiho Choi. 2021. Loki: Long term and key intentions for trajectory prediction. In *Proceedings of the IEEE/CVF International Conference on Computer Vision*. 9803–9812.
 - [22] Zhihao Gu, Yang Chen, Taiping Yao, Shouhong Ding, Jilin Li, Feiyue Huang, and Lizhuang Ma. 2021. Spatiotemporal inconsistency learning for deepfake video detection. In *Proceedings of the 29th ACM international conference on multimedia*. 3473–3481.
 - [23] Zhihao Gu, Yang Chen, Taiping Yao, Shouhong Ding, Jilin Li, and Lizhuang Ma. 2022. Delving into the local: Dynamic inconsistency learning for deepfake video detection. In *Proceedings of the AAAI conference on artificial intelligence*, Vol. 36. 744–752.
 - [24] Zhihao Gu, Taiping Yao, Yang Chen, Shouhong Ding, and Lizhuang Ma. 2022. Hierarchical contrastive inconsistency learning for deepfake video detection. In *European conference on computer vision*. Springer, 596–613.
 - [25] Fabrizio Guillaro, Giada Zingarini, Ben Usman, Avneesh Sud, Davide Cozzolino, and Luisa Verdoliva. 2025. A bias-free training paradigm for more general ai-generated image detection. In *Proceedings of the Computer Vision and Pattern Recognition Conference*. 18685–18694.
 - [26] Xiao Guo, Xiufeng Song, Yue Zhang, Xiaohong Liu, and Xiaoming Liu. 2025. Rethinking Vision-Language Model in Face Forensics: Multi-Modal Interpretable Forged Face Detector. In *Proceedings of the Computer Vision and Pattern Recognition Conference*. 105–116.
 - [27] Zhiyuan He, Pin-Yu Chen, and Tsung-Yi Ho. 2024. Rigid: A training-free and model-agnostic framework for robust ai-generated image detection. *arXiv preprint arXiv:2405.20112* (2024).
 - [28] Jonathan Ho, Ajay Jain, and Pieter Abbeel. 2020. Denoising diffusion probabilistic models. *Advances in neural information processing systems* 33 (2020), 6840–6851.
 - [29] Edward J Hu, Yelong Shen, Phillip Wallis, Zeyuan Allen-Zhu, Yuanzhi Li, Shean Wang, Lu Wang, Weizhu Chen, et al. 2022. Lora: Low-rank adaptation of large language models. *ICLR* 1, 2 (2022), 3.
 - [30] Zhenglin Huang, Jinwei Hu, Xiangtai Li, Yiwei He, Xingyu Zhao, Bei Peng, Baoyuan Wu, Xiaowei Huang, and Guangliang Cheng. 2025. Sida: Social media image deepfake detection, localization and explanation with large multimodal model. In *Proceedings of the Computer Vision and Pattern Recognition Conference*. 28831–28841.
 - [31] Chao Jia, Yinfei Yang, Ye Xia, Yi-Ting Chen, Zarana Parekh, Hieu Pham, Quoc Le, Yun-Hsuan Sung, Zhen Li, and Tom Duerig. 2021. Scaling up visual and vision-language representation learning with noisy text supervision. In *International conference on machine learning*. PMLR, 4904–4916.
 - [32] Yan Ju, Shan Jia, Lipeng Ke, Hongfei Xue, Koki Nagano, and Siwei Lyu. 2022. Fusing global and local features for generalized ai-synthesized image detection. In *2022 IEEE International Conference on Image Processing (ICIP)*. IEEE, 3465–3469.
 - [33] Tero Karras, Samuli Laine, and Timo Aila. 2019. A style-based generator architecture for generative adversarial networks. In *Proceedings of the IEEE/CVF conference on computer vision and pattern recognition*. 4401–4410.
 - [34] Tero Karras, Samuli Laine, Miika Aittala, Janne Hellsten, Jaakko Lehtinen, and Timo Aila. 2020. Analyzing and Improving the Image Quality of StyleGAN. In *Proceedings of the IEEE/CVF Conference on Computer Vision and Pattern Recognition (CVPR)*.
 - [35] Hossein Kashiani, Niloufar Alipour Talemi, and Fatemeh Afghah. 2025. FreqDebias: Towards Generalizable Deepfake Detection via Consistency-Driven Frequency Debiasing. In *Proceedings of the Computer Vision and Pattern Recognition Conference*. 8775–8785.
 - [36] Muhammad Uzair Khattak, Hanoona Rasheed, Muhammad Maaz, Salman Khan, and Fahad Shahbaz Khan. 2023. Maple: Multi-modal prompt learning. In *Proceedings of the IEEE/CVF Conference on Computer Vision and Pattern Recognition*. 19113–19122.
 - [37] Christos Koutlis and Symeon Papadopoulos. 2024. Leveraging representations from intermediate encoder-blocks for synthetic image detection. In *European Conference on Computer Vision*. Springer, 394–411.
 - [38] Kaiqing Lin, Yuzhen Lin, Weixiang Li, Taiping Yao, and Bin Li. 2025. Standing on the shoulders of giants: Reprogramming visual-language model for general deepfake detection. In *Proceedings of the AAAI Conference on Artificial Intelligence*, Vol. 39. 5262–5270.
 - [39] Tsung-Yi Lin, Michael Maire, Serge Belongie, James Hays, Pietro Perona, Deva Ramanan, Piotr Dollár, and C Lawrence Zitnick. 2014. Microsoft coco: Common objects in context. In *European conference on computer vision*. Springer, 740–755.
 - [40] Bo Liu, Fan Yang, Xiuli Bi, Bin Xiao, Weisheng Li, and Xinbo Gao. 2022. Detecting generated images by real images. In *European Conference on Computer Vision*. Springer, 95–110.
 - [41] Haotian Liu, Chunyuan Li, Qingyang Wu, and Yong Jae Lee. 2023. Visual instruction tuning. *Advances in neural information processing systems* 36 (2023), 34892–34916.
 - [42] Huan Liu, Zichang Tan, Chuangchuang Tan, Yunchao Wei, Jingdong Wang, and Yao Zhao. 2024. Forgery-aware adaptive transformer for generalizable synthetic image detection. In *Proceedings of the IEEE/CVF Conference on Computer Vision and Pattern Recognition*. 10770–10780.
 - [43] Zhengzhe Liu, Xiaojuan Qi, and Philip HS Torr. 2020. Global texture enhancement for fake face detection in the wild. In *Proceedings of the IEEE/CVF conference on computer vision and pattern recognition*. 8060–8069.
 - [44] Zhihe Lu, Jiawang Bai, Xin Li, Zeyu Xiao, and Xinchao Wang. 2023. Beyond sole strength: Customized ensembles for generalized vision-language models. *arXiv preprint arXiv:2311.17091* (2023).
 - [45] Laurens van der Maaten and Geoffrey Hinton. 2008. Visualizing data using t-SNE. *Journal of machine learning research* 9, Nov (2008), 2579–2605.
 - [46] Anant Mehta, Bryant McArthur, Nagarjuna Kolloju, and Zhengzhong Tu. 2025. HFMF: Hierarchical Fusion Meets Multi-Stream Models for Deepfake Detection. In *Proceedings of the Winter Conference on Applications of Computer Vision*. 724–733.
 - [47] Dat Nguyen, Nesryne Mejri, Inder Pal Singh, Polina Kuleshova, Marcella Astrid, Anis Kacem, Enjie Ghorbel, and Djamilia Aouada. 2024. Laa-net: Localized artifact attention network for quality-agnostic and generalizable deepfake detection. In *Proceedings of the IEEE/CVF Conference on Computer Vision and Pattern Recognition*. 17395–17405.
 - [48] Alex Nichol, Prafulla Dhariwal, Aditya Ramesh, Pranav Shyam, Pamela Mishkin, Bob McGrew, Ilya Sutskever, and Mark Chen. 2021. Glide: Towards photorealistic

- image generation and editing with text-guided diffusion models. *arXiv preprint arXiv:2112.10741* (2021).
- [49] Utkarsh Ojha, Yuheng Li, and Yong Jae Lee. 2023. Towards universal fake image detectors that generalize across generative models. In *Proceedings of the IEEE/CVF Conference on Computer Vision and Pattern Recognition*. 24480–24489.
- [50] Taesung Park, Ming-Yu Liu, Ting-Chun Wang, and Jun-Yan Zhu. 2019. Gagan: semantic image synthesis with spatially adaptive normalization. In *ACM SIGGRAPH 2019 Real-Time Live! 1–1*.
- [51] Yuyang Qian, Guojun Yin, Lu Sheng, Zixuan Chen, and Jing Shao. 2020. Thinking in frequency: Face forgery detection by mining frequency-aware clues. In *European conference on computer vision*. Springer, 86–103.
- [52] Alec Radford, Jong Wook Kim, Chris Hallacy, Aditya Ramesh, Gabriel Goh, Sandhini Agarwal, Girish Sastry, Amanda Askell, Pamela Mishkin, Jack Clark, et al. 2021. Learning transferable visual models from natural language supervision. In *International conference on machine learning*. PmlR, 8748–8763.
- [53] Anirudh Sundara Rajan, Utkarsh Ojha, Jedidiah Schloesser, and Yong Jae Lee. 2024. Aligned datasets improve detection of latent diffusion-generated images. *arXiv preprint arXiv:2410.11835* (2024).
- [54] Aditya Ramesh, Mikhail Pavlov, Gabriel Goh, Scott Gray, Chelsea Voss, Alec Radford, Mark Chen, and Ilya Sutskever. 2021. Zero-shot text-to-image generation. In *International conference on machine learning*. Pmlr, 8821–8831.
- [55] Jonas Ricker, Denis Lukovnikov, and Asja Fischer. 2024. Aeroblade: Training-free detection of latent diffusion images using autoencoder reconstruction error. In *Proceedings of the IEEE/CVF Conference on Computer Vision and Pattern Recognition*. 9130–9140.
- [56] Robin Rombach, Andreas Blattmann, Dominik Lorenz, Patrick Esser, and Björn Ommer. 2022. High-Resolution Image Synthesis With Latent Diffusion Models. In *Proceedings of the IEEE/CVF Conference on Computer Vision and Pattern Recognition (CVPR)*. 10684–10695.
- [57] Robin Rombach, Andreas Blattmann, Dominik Lorenz, Patrick Esser, and Björn Ommer. 2022. High-resolution image synthesis with latent diffusion models. In *Proceedings of the IEEE/CVF conference on computer vision and pattern recognition*. 10684–10695.
- [58] Andreas Rossler, Davide Cozzolino, Luisa Verdoliva, Christian Riess, Justus Thies, and Matthias Nießner. 2019. Faceforensics++: Learning to detect manipulated facial images. In *Proceedings of the IEEE/CVF international conference on computer vision*. 1–11.
- [59] Ramprasaath R Selvaraju, Michael Cogswell, Abhishek Das, Ramakrishna Vedantam, Devi Parikh, and Dhruv Batra. 2017. Grad-cam: Visual explanations from deep networks via gradient-based localization. In *Proceedings of the IEEE international conference on computer vision*. 618–626.
- [60] Ke Sun, Shen Chen, Taiping Yao, Ziyin Zhou, Jiayi Ji, Xiaoshuai Sun, Chia-Wen Lin, and Rongrong Ji. 2025. Towards general visual-linguistic face forgery detection. In *Proceedings of the Computer Vision and Pattern Recognition Conference*. 19576–19586.
- [61] Chuangchuang Tan, Renshuai Tao, Huan Liu, Guanghua Gu, Baoyuan Wu, Yao Zhao, and Yunchao Wei. 2025. C2p-clip: Injecting category common prompt in clip to enhance generalization in deepfake detection. In *Proceedings of the AAAI Conference on Artificial Intelligence*, Vol. 39. 7184–7192.
- [62] Chuangchuang Tan, Yao Zhao, Shikui Wei, Guanghua Gu, Ping Liu, and Yunchao Wei. 2024. Frequency-aware deepfake detection: Improving generalizability through frequency space domain learning. In *Proceedings of the AAAI Conference on Artificial Intelligence*, Vol. 38. 5052–5060.
- [63] Chuangchuang Tan, Yao Zhao, Shikui Wei, Guanghua Gu, Ping Liu, and Yunchao Wei. 2024. Rethinking the up-sampling operations in cnn-based generative network for generalizable deepfake detection. In *Proceedings of the IEEE/CVF Conference on Computer Vision and Pattern Recognition*. 28130–28139.
- [64] Chuangchuang Tan, Yao Zhao, Shikui Wei, Guanghua Gu, and Yunchao Wei. 2023. Learning on gradients: Generalized artifacts representation for gan-generated images detection. In *Proceedings of the IEEE/CVF Conference on Computer Vision and Pattern Recognition*. 12105–12114.
- [65] Hao Tan, Jun Lan, Senyuan Shi, Zichang Tan, Zijian Yu, Huijia Zhu, Weiqiang Wang, Jun Wan, and Zhen Lei. 2026. Videoveritas: Ai-generated video detection via perception pretext reinforcement learning. *arXiv preprint arXiv:2602.08828* (2026).
- [66] Hao Tan, Jun Lan, Zichang Tan, Ajian Liu, Chuanbiao Song, Senyuan Shi, Huijia Zhu, Weiqiang Wang, Jun Wan, and Zhen Lei. 2025. Veritas: Generalizable deepfake detection via pattern-aware reasoning. *arXiv preprint arXiv:2508.21048* (2025).
- [67] Hao Tan, Zichang Tan, Jun Li, Ajian Liu, Jun Wan, and Zhen Lei. 2025. Recover and Match: Open-Vocabulary Multi-Label Recognition through Knowledge-Constrained Optimal Transport. In *Proceedings of the Computer Vision and Pattern Recognition Conference*. 4650–4660.
- [68] Keyu Tian, Yi Jiang, Zehuan Yuan, Bingyue Peng, and Liwei Wang. 2024. Visual autoregressive modeling: Scalable image generation via next-scale prediction. *Advances in neural information processing systems* 37 (2024), 84839–84865.
- [69] Chung-Ting Tsai, Ching-Yun Ko, I Chung, Yu-Chiang Frank Wang, Pin-Yu Chen, et al. 2024. Understanding and improving training-free ai-generated image detections with vision foundation models. *arXiv preprint arXiv:2411.19117* (2024).
- [70] Sheng-Yu Wang, Oliver Wang, Richard Zhang, Andrew Owens, and Alexei A Efros. 2020. CNN-generated images are surprisingly easy to spot... for now. In *Proceedings of the IEEE/CVF conference on computer vision and pattern recognition*. 8695–8704.
- [71] Tongzhou Wang and Phillip Isola. 2020. Understanding contrastive representation learning through alignment and uniformity on the hypersphere. In *International conference on machine learning*. PMLR, 9929–9939.
- [72] Zhendong Wang, Jianmin Bao, Wengang Zhou, Weilun Wang, Hezhen Hu, Hong Chen, and Houqiang Li. 2023. Dire for diffusion-generated image detection. In *Proceedings of the IEEE/CVF International Conference on Computer Vision*. 22445–22455.
- [73] Monika Wyszoczańska, Oriane Siméoni, Michaël Ramamonjisoa, Andrei Bursuc, Tomasz Trzcziński, and Patrick Pérez. 2024. CLIP-DINOiser: Teaching CLIP a few DINO tricks for open-vocabulary semantic segmentation. In *European Conference on Computer Vision*. Springer, 320–337.
- [74] Zhipei Xu, Xuanyu Zhang, Runyi Li, Zecheng Tang, Qing Huang, and Jian Zhang. 2024. Fakeshield: Explainable image forgery detection and localization via multimodal large language models. *arXiv preprint arXiv:2410.02761* (2024).
- [75] Shilin Yan, Ouxiang Li, Jiayin Cai, Yanbin Hao, Xiaolong Jiang, Yao Hu, and Weidi Xie. 2024. A sanity check for ai-generated image detection. *arXiv preprint arXiv:2406.19435* (2024).
- [76] Zhiyuan Yan, Yuhao Luo, Siwei Lyu, Qingshan Liu, and Baoyuan Wu. 2024. Transcending forgery specificity with latent space augmentation for generalizable deepfake detection. In *Proceedings of the IEEE/CVF Conference on Computer Vision and Pattern Recognition*. 8984–8994.
- [77] Zhiyuan Yan, Jiangming Wang, Peng Jin, Ke-Yue Zhang, Chengchun Liu, Shen Chen, Taiping Yao, Shouhong Ding, Baoyuan Wu, and Li Yuan. 2024. Orthogonal Subspace Decomposition for Generalizable AI-Generated Image Detection. *arXiv preprint arXiv:2411.15633* (2024).
- [78] Zhiyuan Yan, Yandan Zhao, Shen Chen, Mingyi Guo, Xinghe Fu, Taiping Yao, Shouhong Ding, Yunsheng Wu, and Li Yuan. 2025. Generalizing deepfake video detection with plug-and-play: Video-level blending and spatiotemporal adapter tuning. In *Proceedings of the Computer Vision and Pattern Recognition Conference*. 12615–12625.
- [79] Yongqi Yang, Zhihao Qian, Ye Zhu, Olga Russakovsky, and Yu Wu. 2025. D⁺ 3: Scaling Up Deepfake Detection by Learning from Discrepancy. In *Proceedings of the Computer Vision and Pattern Recognition Conference*. 23850–23859.
- [80] Zheng Yang, Ruoxin Chen, Zhiyuan Yan, Ke-Yue Zhang, Xinghe Fu, Shuang Wu, Xiujun Shu, Taiping Yao, Shouhong Ding, and Xi Li. 2025. All Patches Matter, More Patches Better: Enhance AI-Generated Image Detection via Panoptic Patch Learning. *arXiv preprint arXiv:2504.01396* (2025).
- [81] Fulong Ye, Miao Hua, Pengze Zhang, Xinghui Li, Qichao Sun, Songtao Zhao, Qian He, and Xinglong Wu. 2025. DreamID: High-Fidelity and Fast diffusion-based Face Swapping via Triplet ID Group Learning. *arXiv preprint arXiv:2504.14509* (2025).
- [82] Nan Zhong, Yiran Xu, Zhenxing Qian, and Xinpeng Zhang. 2023. Rich and poor texture contrast: A simple yet effective approach for ai-generated image detection. *CoRR* (2023).
- [83] Jiaran Zhou, Yuezun Li, Baoyuan Wu, Bin Li, Junyu Dong, et al. 2024. Freqblender: Enhancing deepfake detection by blending frequency knowledge. *Advances in Neural Information Processing Systems* 37 (2024), 44965–44988.
- [84] Kaiyang Zhou, Jingkang Yang, Chen Change Loy, and Ziwei Liu. 2022. Conditional prompt learning for vision-language models. In *Proceedings of the IEEE/CVF conference on computer vision and pattern recognition*. 16816–16825.
- [85] Kaiyang Zhou, Jingkang Yang, Chen Change Loy, and Ziwei Liu. 2022. Learning to prompt for vision-language models. *International Journal of Computer Vision* 130, 9 (2022), 2337–2348.
- [86] Ziyin Zhou, Yungpeng Luo, Yuanchen Wu, Ke Sun, Jiayi Ji, Ke Yan, Shouhong Ding, Xiaoshuai Sun, Yunsheng Wu, and Rongrong Ji. 2025. AIGI-Holmes: Towards Explainable and Generalizable AI-Generated Image Detection via Multimodal Large Language Models. *arXiv preprint arXiv:2507.02664* (2025).
- [87] Beier Zhu, Yulei Niu, Yucheng Han, Yue Wu, and Hanwang Zhang. 2023. Prompt-aligned gradient for prompt tuning. In *Proceedings of the IEEE/CVF International Conference on Computer Vision*. 15659–15669.
- [88] Yijie Zhu, Yibo Lyu, Zitong Yu, Rui Shao, Kaiyang Zhou, and Liqiang Nie. 2025. EmoSym: A Symbiotic Framework for Unified Emotional Understanding and Generation via Latent Reasoning. In *Proceedings of the 33rd ACM International Conference on Multimedia*.
- [89] Yijie Zhu, Rui Shao, Ziyang Liu, Jie He, Jizhihui Liu, Jiuru Wang, and Zitong Yu. 2026. H-GAR: A Hierarchical Interaction Framework via Goal-Driven Observation-Action Refinement for Robotic Manipulation. In *Proceedings of the AAAI Conference on Artificial Intelligence*.
- [90] Yijie Zhu, Lingsen Zhang, Zitong Yu, Rui Shao, Tao Tan, and Liqiang Nie. 2025. UniEmo: Unifying Emotional Understanding and Generation with Learnable Expert Queries. *arXiv preprint arXiv:2507.23372* (2025).